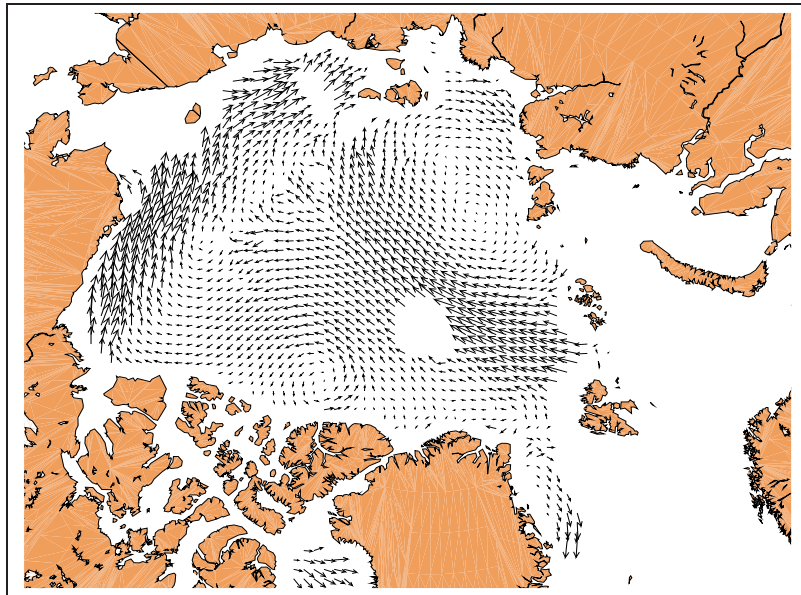


# Validation and Monitoring of the OSI SAF Low Resolution Sea Ice Drift Product

OSI-405



OSI SAF 48h sea ice drift field retrieved from AMSR-E imagery. Drift is from November, 22<sup>nd</sup> to 24<sup>th</sup> 2008.

Version 2 — March 2010

Thomas Lavergne



**Documentation Change Record:**

Version	Date	Author	Description
v0.9	03.12.2008	TL	Initial version, before review
v1	05.02.2009	TL	Amended after PCR comments
v2	15.03.2010	TL	Include more in-situ data sources, change the collocation method and extend validation time period.

# Table of contents

## Table of contents

### List of Figures

<b>1 Introduction</b>	<b>1</b>
1.1 Overview . . . . .	1
1.2 Glossary . . . . .	2
<b>2 Validation dataset</b>	<b>3</b>
2.1 In-situ trajectories . . . . .	3
2.2 Remarks on the validation dataset . . . . .	5
2.3 Acknowledgements . . . . .	5
2.4 Geographical overview of the validation dataset . . . . .	6
<b>3 Validation methodology</b>	<b>7</b>
3.1 Variables to be validated . . . . .	7
3.2 Reformatting of the validation dataset . . . . .	7
3.3 Collocation strategies . . . . .	7
3.4 Representativeness error . . . . .	8
3.5 Graphs and statistical measures . . . . .	9
<b>4 Results of validation</b>	<b>11</b>
4.1 Graphs and analysis . . . . .	11
4.2 Comparison to other datasets . . . . .	14
4.3 Discussion and conclusion . . . . .	14
<b>5 Temporal monitoring of the ice drift products</b>	<b>16</b>
5.1 Discussion on the distribution period . . . . .	16
5.2 Availability of input swath data and impact for use of the products . . . . .	19
<b>6 Conclusion</b>	<b>21</b>
<b>References</b>	<b>23</b>

# List of Figures

1	Location of the ITPs as of January 14 <sup>th</sup> 2010 . . . . .	4
2	Trajectories of the validation drifters . . . . .	6
3	Validation graphs for ice drift products . . . . .	12
4	Validation graphs for ice drift products — continued . . . . .	13
5	Monitoring of the density of valid vectors in the ice covered cells. . . . .	17
6	Monitoring of the average MCC for computed vectors . . . . .	17
7	Monitoring of the density of corrected vectors . . . . .	18
8	Monitoring of the number of missing vectors due to missing input swath . . . . .	19

# 1. Introduction

## 1.1 Overview

Sea ice drift products for Northern Hemisphere are processed at the High Latitude center of the Ocean & Sea Ice Satellite Application Facility (EUMETSAT OSI SAF). Those datasets are introduced and documented in a dedicated Product User's Manual (PUM, Lavergne and Eastwood 2010) and in an Algorithm Theoretical Basis Document (ATBD, Lavergne et al. 2009) that can both be found on <http://saf.met.no>. The High Latitude processing facility (HL centre) is jointly operated by the Norwegian and Danish Meteorological Institutes.

See <http://saf.met.no> for real time examples of the products as well as updated information. The latest version of this document can also be found there. General information about the OSI SAF is given at <http://www.osi-saf.org>.

This Validation and Monitoring report only deals with the OSI-405 low resolution sea ice drift product. The medium resolution ice drift product based on AVHRR imagery, OSI-407, is documented in a dedicated report.

The aims of this report are several:

1. To document the level of agreement between the OSI SAF low resolution sea ice drift product and ground-based truth. Various graphs displaying the match between the satellite product and the in-situ datasets should give (qualitative) confidence in using the product.
2. To report quantitative estimates of errors and uncertainties in the product. Particularly, the bias and uncertainty covariance matrix is computed. It is important that each single-sensor and the multi-sensor products are validated separately so that users can have error estimates for the product they choose to use.
3. To present temporal monitoring of the sea ice drift product in terms of geographical coverage, and number of daily missing vectors.

While items number 1 and 2 deal with comparing the product against a 'reference' dataset, item 3 is purely a monitoring activity that analyses the product on its own.

Chapter 2 presents the datasets used as validation data while chapter 3 documents the validation strategy and, particularly, the way collocation is handled. Chapter 4 provides detailed, graphical and quantitative analysis of the validation results. Chapter 5 proposes graphical analysis of temporal monitoring. We conclude in chapter 6.

Note that the OSI SAF low resolution sea ice drift product will not be introduced in any depth in this report. Refer to the PUM and <http://saf.met.no> for information on the algorithms, processing schemes and data format.

Let us nonetheless remind that the OSI SAF low resolution ice drift product comes as daily vector fields obtained by processing low-resolution satellite signal from, among others, AMSR-E, SSM/I and ASCAT. It is computed on a Northern Hemisphere grid and delivered from October, 1st to April, 30th every year. Summer ice drift is indeed not as straightforward from those sensors. It is a 2 days (48 hours) ice drift product on a 62.5 km resolution polar stereographic grid. Both single and multi sensor products are distributed.

## 1.2 Glossary

AARI	Arctic and Antarctic Research Institute
AWI	Alfred Wegener Institute
ASCAT	Advanced SCATterometer
AVHRR	Advanced Very High Resolution Radiometer
AMSR-E	Advanced Microwave Scanning Radiometer for EOS
CDOP	Continuous Development and Operations Phase
DMI	Danish Meteorological Institute
DMSP	Defense Meteorological Satellite Program
IABP	International Arctic Buoy Program
IBCAO	International Bathymetric Chart of the Arctic Ocean
ITP	Ice Tethered Profiler
GPS	Global Positioning System
HL	High Latitudes
met.no	Norwegian Meteorological Institute
NetCDF	network Common Data Format
NH	Northern Hemisphere
NP	North Pole
SAF	Satellite Application Facility
SSM/I	Special Sensor Microwave/Imager

## 2. Validation dataset

In this section, we introduce the ice motion datasets that constitute our best estimate of the ground truth and that is used as reference to validate the OSI SAF low resolution sea ice drift dataset.

Several data sources are available for validating an ice drift product and they can be sorted into three groups:

1. **Trajectories of in-situ ice drifters.** Historically, this is the main validation data source. A fair number of buoys are indeed deployed in the ice covered ocean to measure atmospheric, cryospheric or oceanic variables (e.g. Mean Sea Level Pressure, ice thickness or temperature and salinity profiles of the ocean). Of interest to us is the fact that they regularly and automatically report their position via the Argos system or by transmitting GPS positions as part as their data stream. Drifting ships (like the Tara) or manned stations (NP-35, NP-36, etc...) also constitute good opportunities to get ice trajectory data, sometimes in near-real-time.
2. **High resolution satellite based ice drift datasets.** Those are processed from high resolution satellite images (e.g. ENVISAT SAR or AVHRR). Those products are not 'ground truth' but are assumed to present much less deviations to truth than the low resolution ice drift datasets.
3. **Moored Doppler-based velocity measures from under the ice.** This source of data presents three major disadvantages. Firstly, they are Eulerian measures of instantaneous velocity, a quantity that is not directly comparable to satellite-based ice displacement vectors. Second, they do not transmit data in near-real-time and are thus not suitable for daily monitoring of a product. Finally, they are often located in coastal areas where the retrieval of sea ice drift from low resolution sensors is challenged by the proximity to land.

For the validation exercise reported in this document, only in-situ trajectories have been used as reference dataset. SAR-based ice drift as produced, for example, at the Danish Technical University can hopefully be included at a later stage.

### 2.1 In-situ trajectories

#### 2.1.1 Ice Tethered Profilers

The Ice Tethered Profilers (ITP) platforms are advanced autonomous drifting instrument that are designed to measure temperature and salinity profiles in the ocean under sea ice. As part of its daily data stream, each ITP transfers hourly unfiltered GPS locations. As of

January 2010, there are 20 active ITPs in the Arctic Ocean that form a high quality validation dataset, especially for the Beaufort Sea, Canadian Basin and Fram Strait.

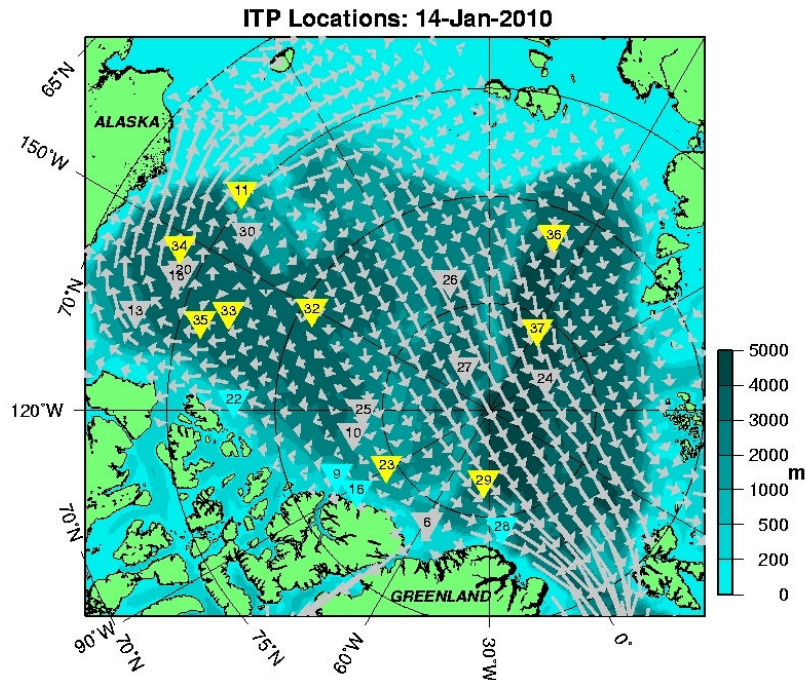


Figure 1: Latest locations of all active ITPs. Systems that are presently providing location and profile data are in yellow, those that are providing locations only (profiler status uncertain) are in cyan, and those that have not transmitted data for over one month are plotted in gray. Also shown are annual ice drift vectors from IABP on IBCAO bathymetry.

Figure (1) and its caption were directly extracted from <http://www.whoi.edu/itp> on January 14<sup>th</sup> 2010 and display the position of the ITPs at that date.

The ASCII formatted level 1 raw data position files (`itpNrawlocs.dat`) for all ITPs were downloaded from the FTP server at Woods Hole Oceanographic Institution and processed to extract ice drift vectors.

### 2.1.2 Tara

The Tara schooner (<http://www.taraexpeditions.org>) has been one of the flagships of the Developing Arctic Modelling and Observing Capabilities for Long-term Environmental Studies (DAMOCLES, [www.damocles-eu.org](http://www.damocles-eu.org)) project. Its now famous drift started in September 2006. It followed the transpolar drift motion and was released from the ice in the first days of January 2008. All along its 500 days drift, the ship's position was recorded via Argos and in a sub-hourly GPS log.

Although it provides only one vector per day, moreover only until January 3rd 2008, this dataset is relevant since it samples a geographical region (Transpolar Drift and Fram Strait) that is not very often sampled by the other drifters.

### 2.1.3 Russian manned polar stations

GPS trajectory logs for the Russian manned stations NP-35, NP-36 and NP-37 were made available by the Arctic and Antarctic Research Institute (AARI). The drift of NP-35 lasted from September 2007 to July 2008. Its GPS trajectory was not available in near-real-time. NP-36 was deployed in September 2008 and recovered August 2009. NP-37 was deployed September 2009. Positions for NP-36 and NP-37 were made available in near-real-time from the AARI web site <http://www.aari.nw.ru>.

As for the Tara, the NP stations provides ice drift vectors in a region not often sampled by the ITPs, namely the Nansen Basin.

### 2.1.4 Buoy array deployed by Brümmer *et al.*

In the context of the DAMOCLES project, an array of 16 CALIB buoys was deployed in April 2007 in the central Arctic. They were dropped from an airplane within a square pattern of  $400 \times 400$  km centred on the Tara (see section 2.1.2). Trajectories are originally recorded via the Argos doppler positioning system, but the dataset used in the present report have been pre-processed and quality checked at the University of Hamburg. They are thus expected of much higher quality than raw Argos (Dr. Gerd Müller, personal communication).

## 2.2 Remarks on the validation dataset

Although we tried to use as many good quality drifters as possible, entire regions covered by the OSI SAF ice drift product grid are not sampled by our validation dataset. See, for reference, Figure (2). Two such regions are the Baffin and Hudson Bay for which it was not possible to obtain trajectories in the validation period we have been covering. Some buoys are released every year in the Nares Strait. However, most of them sink due to unstable ice conditions in the strait or Baffin Bay at that period.

## 2.3 Acknowledgements

The Ice-Tethered Profiler data were collected and made available by the Ice-Tethered Profiler Program based at the Woods Hole Oceanographic Institution <http://www.whoi.edu/itp>.

GPS-located data from Russian stations (NP-35, NP-36, NP-37) were kindly provided by the Arctic and Antarctic Research Institute (AARI, <http://www.aari.ru>) of Roshydromet, PIs Vladimir Sokolov and Vasily Smolyanitsky.

The GPS trajectory of the Tara was kindly made available by the DAMOCLES project.

The preprocessed trajectories of the 16 CALIB buoys array were kindly offered by Dr. Burghard Brümmer and Dr. Gerd Müller, both from the Meteorological Institute at University of Hamburg.

## 2.4 Geographical overview of the validation dataset

Figure (2) displays a graphical overview of the in-situ trajectories that were used in the validation period. Ice Tethered Profilers, NP-35, NP-36 the buoy array and the Tara are all included. Red color is used for the GPS positions and blue for the one using Argos.

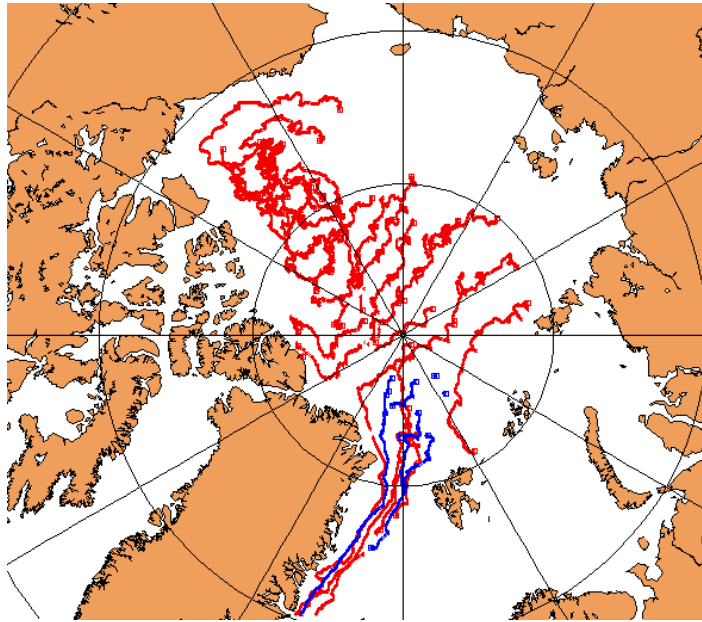


Figure 2: Trajectories of the validation drifters (ITPs, Tara and NP-35) in the period 1<sup>st</sup> October to 30<sup>th</sup> April in 2006-2007, 2007-2008 and 2008-2009.

## 3. Validation methodology

The validation strategy is introduced in this chapter. It covers the re-formatting of the trajectories and the collocation with the sea ice drift product. We also present the graphs and statistical properties that will be displayed and commented upon in chapter 4.

### 3.1 Variables to be validated

As introduced in the sea ice drift PUM, an ice drift vector is fully described with 6 values: the geographical position of the start point ( $lat_0$  and  $lon_0$ ), the start time of the drift ( $t_0$ ), the position of the end point of the drift ( $lat_1$  and  $lon_1$ ) as well as the end time of the drift ( $t_1$ ).

However, the primary variables the ice drift processing software optimizes are  $dX$  and  $dY$ , the components of the displacement vector along the X and Y axes of the product grid. Those are thus the two variables we are aiming at validating.

### 3.2 Reformatting of the validation dataset

In any validation exercise, especially if making use of a broad range of data sources, one is confronted to new and varying formats. Most of the times, trajectories from in-situ drifters are available in an ASCII format, proposing one position and time stamp per line. The various formats for the time information, in particular, as well as the ordering of columns make it challenging to design a unique software package to read all those files.

A first step of this validation effort has thus been the design of dedicated software routines to read the observation files, extract the portion of the trajectory that fits the time span of the OSI SAF ice drift product file and dump the validation data in a NetCDF formatted file.

### 3.3 Collocation strategies

In order to compare the OSI SAF sea ice drift product with the validation trajectories, they need to be collocated one with the other. Collocation is the act of selecting or transforming one or both datasets so that they represent the same quantity, at the same time and at the same geographical location.

Because the OSI SAF ice drift product comes with two flavours of time information (refer to PUM, section *Time information*), two validation exercises are conducted:

- One using a 2D collocation, in which the satellite product is considered representing a drift from day  $D@1200\text{ UTC}$  to  $(D+2)@1200\text{ UTC}$ , uniformly over the grid.

- One with a 3D collocation, in which the position dependent start and end times are used (found in datasets dt0 and dt1, in the product file).

The reason for having those two validation strategies is that some users might wish (or have to) ignore the accurate timing information provided with each vector. Using only the central times, these users need to know if the uncertainty estimates are to be enlarged and, if so, by which amount.

### 3.3.1 2D collocation

The in-situ drift vector is defined by first selecting the start and end position record in their trajectory. Those are the ones closest (in time) to *1200 UTC*, on both dates. From those 2 positions,  $dX_{ref}$  and  $dY_{ref}$  are computed. The product  $dX_{prod}$  and  $dY_{prod}$  are those of the nearest-neighbour in the product grid.

### 3.3.2 3D collocation

The in-situ start (end) point is searched for along the trajectory: each record is remapped into the product grid where a product start (end) time is computed by bilinear interpolation from the 4 encompassing grid points. Because the records are ordered chronologically, it is possible to stop searching as soon as both start and end in-situ records are selected. As in the 2D collocation, they define the 'truth' displacement components:  $dX_{ref}$  and  $dY_{ref}$ . The components for the product ( $dX_{prod}$  and  $dY_{prod}$ ) are selected as those of the nearest-neighbour in the product grid.

### 3.3.3 Remarks

- In early versions of this validation exercise, the spatial collocation was achieved by bilinear interpolation of the 4 neighbouring vectors from the product grid to the position of the reference vector. Further investigations confirmed that this method could lead to artificially good validation statistics, since part of the noise in the product was averaged out in this process.
- The following criteria are used for accepting a collocation pair:
  - The time difference in one of the start or end point must be less than 3 hours;
  - The distance to the nearest neighbour must be inside 30 km radius from the start of reference vector.

## 3.4 Representativeness error

Although we only use high quality buoy position data and although the collocation methods and parameters are quite stringent, a possibly high and mostly uncontrolled source of error resides in the representativeness mismatch between the scales sampled by the buoy and the satellite product.

A buoy indeed samples the motion of the ice floe it was deployed over. Although investigators in field campaigns tend to choose rather large floes for limiting the risk of the

buoy disappearing too rapidly, the size and shape of the floe can change with time through collision or breaking events.

On the other hand, the satellite ice drift product samples the motion of a much larger area of the sea ice surface that is close to 12000 km<sup>2</sup>. The mismatch between the two scales of motion contributes to part of the error budget and it is not possible to separate this representativeness error from the measurement error of the satellite product.

## 3.5 Graphs and statistical measures

As introduced in section 3.1, this report is mostly interested in validating drift components  $dX$  and  $dY$ . We concentrate on two comparison exercises for reporting validation results for those variables.

### 3.5.1 Product vs Reference

In this type of graph, the x-axis is the truth and the y-axis is the estimate given by the product. In an ideal comparison, all (truth,product) pairs are aligned on the 1-to-1 line. The spread around this ideal line can be expressed by the statistical correlation coefficient  $\rho(\text{Reference, Product})$ , noted  $\rho(R, P)$ . If, at the same time, this correlation is close to 1 and the parameters of the regression line are close to 1 ( $\alpha$ , slope) and 0 ( $\beta$ , intercept), then the match between the truth and the product is satisfactory.

In this report, a unique graph (and statistical values) is produced for  $dX$  and  $dY$  at the same time. This means that the pairs appearing on the graphs are both  $(dX_{\text{ref}}, dX_{\text{prod}})$  and  $(dY_{\text{ref}}, dY_{\text{prod}})$ . This also implies that errors in  $dX$  and  $dY$  are considered globally independent, an assumption that is validated using the graphs introduced in the next section.

### 3.5.2 Error in $dY$ vs error in $dX$

In this type of graph, the x-axis is the error in  $dX$ , that is  $dX_{\text{prod}} - dX_{\text{ref}}$  (noted  $\varepsilon(dX)$ ) and the y-axis is the error in  $dY$ , that is  $dY_{\text{prod}} - dY_{\text{ref}}$ , noted  $\varepsilon(dY)$ . This graph is a more interesting approach for presenting the validation data than the one presented in the previous section.

Indeed, such a graph permits giving quantitative estimates for:

- the statistical bias<sup>1</sup> in both components:  $\langle \varepsilon(dX) \rangle$  and  $\langle \varepsilon(dY) \rangle$ ;
- the statistical standard deviation of the errors in both components:  $\sigma(dX)$  and  $\sigma(dY)$ ;
- the statistical correlation between the errors in both components:  $\rho(\varepsilon dX, \varepsilon dY)$ .

The last three quantities enter the error covariance matrix  $C_{\text{obs}}$  which is of prime importance to any data assimilation scheme. It is important to note the difference between the correlation coefficient introduced in this section and the one from section 3.5.1.  $\rho(\varepsilon dX, \varepsilon dY)$  assesses if the errors in the two components of the drift vector are correlated or not.  $\rho(R, P)$  assesses if the product (seen as a sample) is close to a linear combination of the reference dataset (seen as a sample too).

---

<sup>1</sup> $\langle x \rangle$  is the average of  $x$ .

---

In any case, those are statistical measures of the errors. They can only give average uncertainties estimates and result in a unique set of numbers (those populating  $C_{obs}$ ) to be used for an extended period of time (all distribution year round) and for the whole extent of the Northern Hemisphere grid.

## 4. Results of validation

### 4.1 Graphs and analysis

Figure (3) and Figure (4) introduce selected validation graphs for various single-sensor OSI SAF sea ice drift products as well as for the multi-sensors dataset. For all plots, the geographical region being validated is the Northern Hemisphere and the validation period includes all product files whose start date is between October, 1st and April, 30th in 2006-2007, 2007-2008 and 2008-2009.

On "Error( $dY$ ) vs Error( $dX$ )" graphs (left column in Figure (3) and all in Figure (4)), the red (green) thick line encompasses a region of the bivariate error PDF representing 0.68 (0.95) probability of occurrence of a validation pair. Corresponding dashed lines are drawn for the  $1.5\sigma$  and  $2.5\sigma$  ellipses, which are known to delineate 0.68 and 0.95 probability regions in the case of a bivariate normal distribution with parameters  $\langle \varepsilon(dX) \rangle$ ,  $\langle \varepsilon(dY) \rangle$ ,  $\sigma(dX)$ ,  $\sigma(dY)$  and  $\rho(\varepsilon dX, \varepsilon dY)$  (Lavergne et al. 2006, Appendix G). A black plus (+) symbol is located at the centre point of the PDF, namely  $(\langle \varepsilon(dX) \rangle, \langle \varepsilon(dY) \rangle)$ .

On "Product vs Reference" graphs (right column in Figure (3)) each validation pair (one for  $dX$  and one for  $dY$ ) are plotted in a 1-to-1 scatterplot. The solid line is the regression line (whose coefficients are entered as labels in the plot area).

Figure (3) and Figure (4) are a simple and effective way of presenting the validation results and get a good impression of the quality of each product. First, it can be noted that all products are mostly non biased. The magnitudes of  $\langle \varepsilon(dX) \rangle$ ,  $\langle \varepsilon(dY) \rangle$  are indeed small (a couple of 100 metres) in comparison to the standard deviations (a couple of 1000 metres). This is an important result when it comes to using the products in assimilation exercises. The bias in the Y component of the drift is usually larger than for the X component. Besides, it is quite consistently negative which indicates that the satellite product has a smaller drift magnitude than the reference dataset. Kwok et al. (1998) (section 3.2, p. 8203) wrote a detailed investigation of a similar bias in their ice drift product. Such a thorough analysis has not yet been performed for the OSI SAF product and we are left with referring to Kwok's analysis and to following versions of this report, especially when SAR ice drift vectors enter the reference datasets.

It also clearly appears from an analysis of Figure (3) that the method implemented in the OSI SAF chain results in a limited uncertainty. Displacement errors (in terms of standard deviation) are small (maximum 4.5 km,  $1/3$  of image pixel size). Those errors are small despite no special treatment has been implemented for correcting the satellite geolocation uncertainty which might contribute to a fair amount for sensors like SSM/I and AMSR-E (see for example Wiebe et al. 2008).

Another interesting result is that errors in  $dX$  and  $dY$  are mostly uncorrelated. This translates into having the red and green ellipses of the bivariate PDF aligned with the carte-

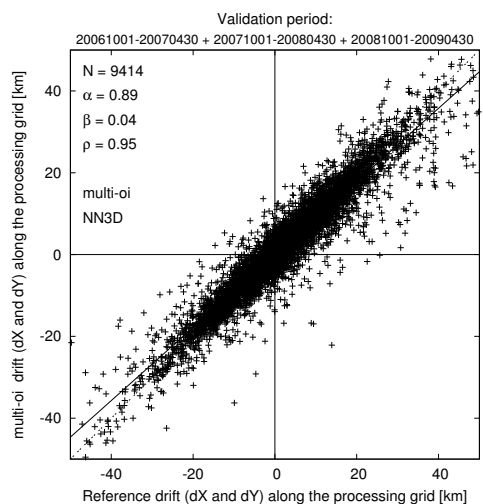
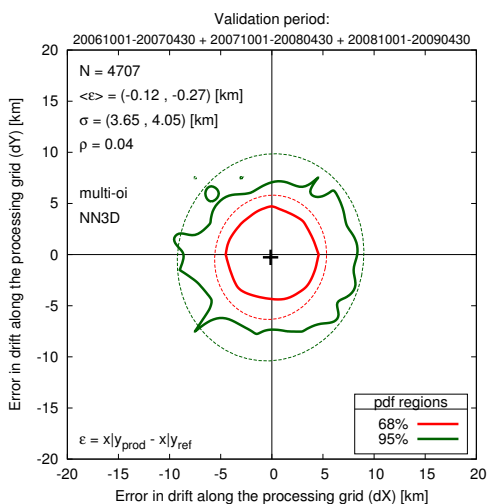
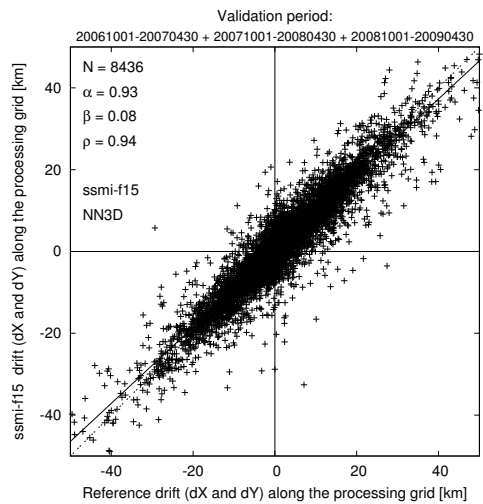
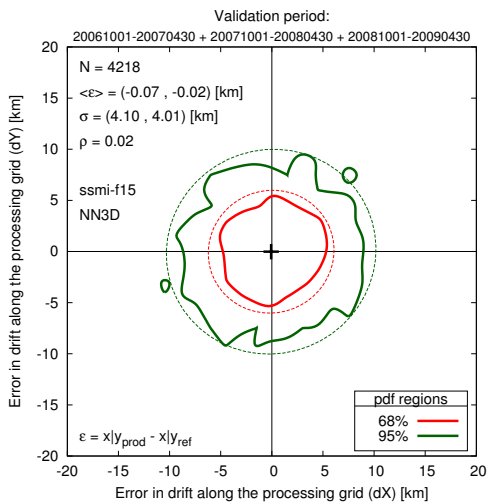
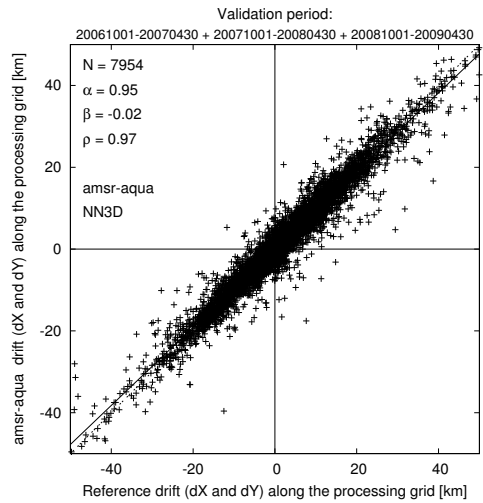
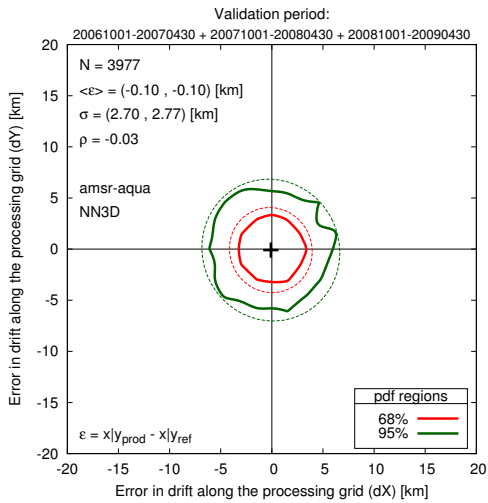


Figure 3: Selected validation graphs for AMSR-E (top row), SSM/I 'F15' (middle row) and merged (multi-oi) (bottom row) products. All pertain to the 3D collocation setup and October 1<sup>st</sup> to April 30<sup>th</sup> in 2006-2007, 2007-2008 and 2008-2009 period. Left (right) column presents "error(dY) vs error(dX)" ("product vs reference") types of graphs. N is the number of validation pairs.

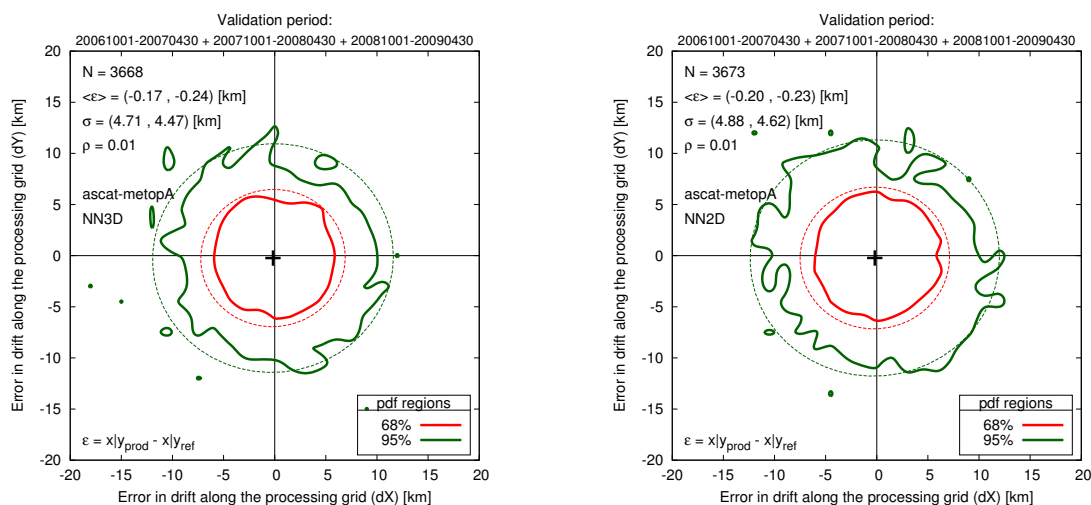


Figure 4: Validation graph for ASCAT product. The left (right) panel contains results for the 3D (2D) collocation methods.

sian axes of the graphs. The observation error covariance matrix  $C_{obs}$  can most probably be considered a diagonal matrix as a first approach. Note however that all necessary information is provided in this report to use a non-diagonal  $C_{obs}$ .

Most assimilation techniques imply (or are used in) a Gaussian model for the error distribution. The close match between the solid and dashed red and green curves on Figure (3) and Figure (4) are a qualitative assessment that the statistical error distribution is not far from a perfect bivariate Gaussian model. A quantitative assessment would require computing bivariate tail and Kurtosis statistics which was not performed in this report.

The analysis conducted so far indicates that the error distribution (when spatially and temporally averaged) can be quite safely approximated by a 0 mean, uncorrelated, bivariate Gaussian probability model. Only the standard deviations  $\sigma(dX)$  and  $\sigma(dY)$  are to be adapted when choosing from the set of single- and multi- sensor ice drift products.

Indeed, when it comes to ranking the products, one of them seems to compare much better with the validation dataset. The sea ice drift product retrieved from AMSR-E (37GHz channels) presents, by far, the smallest values for both  $\sigma(dX)$  and  $\sigma(dY)$ . This limited range of errors also translates in the high correlation coefficient ( $\rho = 0.97$ ) and good regression line for this product (right column, first row in Figure (3)). This can also be visualized by looking at the vector field itself which, most of the times, looks less noisy than the ones from other instruments.

This higher quality might be explained by several factors, including the smaller footprint/spacing of the two 37 GHz channels on board AMSR-E (see the PUM) and the better temporal stability of their intensity patterns (compared to, e.g., those at 85GHz on SSM/I). In any case, the ice drift product from AMSR-E allows statistical standard deviations of 2.70 km (2.77 km) and is the product comparing best to the reference dataset. The main drawback of the AMSR-E product, however, is the average stability of the Aqua satellite platform which causes quite frequent delays or interruptions in the reception of input swath data at the OSI SAF HL processing centre. As a consequence, it is not rare that the grid is incompletely filled or that the product is missing for one or more days.

Ice drift datasets from other sources (SSM/I and ASCAT) have approximately all equivalent quality, with statistical standard deviations in the range 4.0 – 4.5 km.

## 4.2 Comparison to other datasets

Kwok et al. (1998), for example, report standard deviations of 8.9 km (10.8) and 9.9 (11.2) for SSM/I 85 GHz V. pol.  $dX$  ( $dY$ ) and H. pol.  $dX$  ( $dY$ ) products, respectively. This is for a 3 days product in the central Arctic. For their 1 day dataset in the Fram Straits and Baffin Bay, those values are 5.3 km (4.3) and 6.0 (4.7) respectively. Those values are extracted from Table 2, p. 8196. To be fair, one should mention that the validation exercise in Kwok et al. (1998) was performed against IABP buoys and using a 2D-type collocation (see our section 3.3.1). IABP buoys are mainly tracked with Argos positioning, which are more uncertain. Those statistics would thus better be compared with those in our Table (2). This being said, Kwok et al. do not state clearly either that they provide the accurate  $t_0$  and  $t_1$  time information which are needed for using their product in a 3D collocation strategy.

Ezraty et al. (2007) propose a theoretical derivation of the variance induced by the pixel length in the Maximum Cross Correlation technique. They deduce the value of  $\delta^2/6$  for the variance in  $dX$  and  $dY$ , where  $\delta$  is the pixel's length. Although the OSI SAF ice drift products are not derived using the MCC (see PUM), it is comforting to note that the equivalent standard deviation for the 12.5 km resolution pixels we are processing is 5.1 km. This is only a theoretical estimate which does not include other uncertainty sources such as any atmospheric contamination, satellite geolocation errors or non accuracy of the start and end time of the drift vectors. It is even more so satisfactory to document standard deviations for the OSI SAF products below this theoretical value.

Error statistics reported for the various IFREMER datasets (QuikSCAT-SSM/I merged and AMSR-E 89 GHz) as well as by Haarpaintner (2006) are not obviously compared with our values as they are computed for the North-South and East-West components of the drift vectors. Those components exhibit non linear, latitude dependent relationships to the  $dX$  and  $dY$  we are validating. Note, however, that only the AMSR-E (89 GHz) from IFREMER and the QuikSCAT product of Haarpaintner (2006) have a time span of 2 days like the OSI SAF product. The merged SSM/I and QuikSCAT dataset delivered by IFREMER is a 3 days ice drift product.

## 4.3 Discussion and conclusion

The validation statistics for all the OSI SAF low resolution ice drift products are summarized in Table (1) (3D collocation) and Table (2) (2D collocation).

On top of the analysis conducted so far from Figure (3) and Figure (4), the most interesting comparison between those two tables is the slight degradation of the statistics from the 3D to the 2D collocation. For example, the AMSR-E standard deviations grow from 2.70 (2.77) km to 3.11 (3.05) km. Neglecting the information on  $t_0$  and  $t_1$  thus led to enlarging the uncertainties in each drift component by roughly 350 meters. The other products show a similar (although more limited) pattern. The multi-sensor product exhibits no sensitivity to the use (or not) of the extra temporal information. This is not surprising as the merging

Product	$\langle \varepsilon(\mathbf{d}X) \rangle$	$\langle \varepsilon(\mathbf{d}Y) \rangle$	$\sigma(\mathbf{d}X)$	$\sigma(\mathbf{d}Y)$	$\rho(\mathbf{d}X, \mathbf{d}Y)$	$\alpha$	$\beta$	$\rho(R, P)$
amsr-aqua	-0.10	-0.10	<b>2.70</b>	<b>2.77</b>	-0.03	0.95	-0.02	0.97
ssmi-f15	-0.07	-0.02	<b>4.10</b>	<b>4.01</b>	+0.02	0.93	+0.08	0.94
ascametopA	-0.17	-0.24	<b>4.71</b>	<b>4.47</b>	+0.01	0.92	-0.05	0.92
multi-oi	-0.12	-0.27	<b>3.65</b>	<b>4.05</b>	+0.04	0.89	+0.04	0.95

Table 1: Statistical results for validation of the ice drift product in Northern Hemisphere for period October, 1<sup>st</sup> to April, 30<sup>th</sup> in 2006-2007, 2007-2008 and 2008-2009. Those results pertain to the 3D collocation. In the 6<sup>th</sup> column,  $\rho(\mathbf{d}X, \mathbf{d}Y)$  is a shortened notation of  $\rho(\varepsilon(\mathbf{d}X), \varepsilon(\mathbf{d}Y))$ .

Product	$\langle \varepsilon(\mathbf{d}X) \rangle$	$\langle \varepsilon(\mathbf{d}Y) \rangle$	$\sigma(\mathbf{d}X)$	$\sigma(\mathbf{d}Y)$	$\rho(\mathbf{d}X, \mathbf{d}Y)$	$\alpha$	$\beta$	$\rho(R, P)$
amsr-aqua	-0.09	-0.12	<b>3.11</b>	<b>3.05</b>	-0.06	0.95	-0.02	0.96
ssmi-f15	-0.07	-0.01	<b>4.41</b>	<b>4.24</b>	+0.02	0.92	+0.09	0.93
ascametopA	-0.20	-0.23	<b>4.88</b>	<b>4.62</b>	+0.01	0.92	-0.05	0.92
multi-oi	-0.12	-0.27	<b>3.65</b>	<b>4.05</b>	+0.04	0.89	+0.04	0.95

Table 2: Statistical results for validation of the ice drift product in Northern Hemisphere for period October, 1<sup>st</sup> to April, 30<sup>th</sup> in 2006-2007, 2007-2008 and 2008-2009. Those results pertain to the 2D collocation. In the 6<sup>th</sup> column,  $\rho(\mathbf{d}X, \mathbf{d}Y)$  is a shortened notation of  $\rho(\varepsilon(\mathbf{d}X), \varepsilon(\mathbf{d}Y))$ .

procedure implemented in the OSI SAF chain does not allow for book-keeping the time information of each vector (see PUM). As a result are the statistics for the 2D and 3D collocations identical.

This enlargement of the error statistics is, however, damped by the high level of averaging occurring in our validation exercise, spatially and temporally. On a single case basis, like when a circular motion pattern is induced by a moving atmospheric low pressure, the  $t_0$  and  $t_1$  are quite significant and should not be neglected, as illustrated in Lavergne et al. 2008.

Finally, it should be noted that the statistical results and particularly the standard deviations and bias are quite depending on the collocation methodology and on the choice of reference data to enter the validation database. Indeed, the standard deviation for the amsr-aqua product (3D collocation) over the same period is only 2.56 (2.59) km when the Argos trajectories from the buoy array (section 2.1.4) are not included. Further studies are needed for providing an accurate value for the observation uncertainties of the ice drift products to be used in data assimilation applications.

# 5. Temporal monitoring of the ice drift products

## 5.1 Discussion on the distribution period

As for the IFREMER sea ice drift products, the distribution period for the OSI-405 product is from 1<sup>st</sup> October to 30<sup>th</sup> April each year. In this chapter, we provide evidence that it is a relevant choice but also that further investigation could allow to slightly extend this period.

Figure (5) displays the temporal evolution of the density of valid vectors in the sea ice covered cells in the product grid for the various OSI SAF products (single sensor and multi sensors). It covers the time period from 1<sup>st</sup> September 2006 to 31<sup>st</sup> May 2009, hence one month before and after the period in which the ice drift products are distributed (marked with grey background colors). There is no ASCAT product in 2006-2007 since the Metop-A platform was launched in October 2006 and that it took some time before calibrated data could be accessed for science applications.

The density of valid vectors is defined as the ratio between the number of grid locations where an ice drift vector is provided on the number of grid locations where the ice drift retrieval was attempted. This number includes all grid points that are on ice but not too close to the ice edge or coast and that are not missing (e.g. around the polar observation hole or in the vicinity of a missing swath). This density number can thus be seen as a success rate for the OSI SAF ice drift algorithm: how often does it succeed in delivering a vector compared to the number of times it tries matching satellite images. It is not clear the value we report here can be compared one-to-one to those appearing in the Figure (1) of Ezraty et al. (2008).

Nevertheless, the average density level reported on Figure (5) are most of the time around 0.9 for single sensor products and very close to 1.0 for the multi sensor product. Those values confirm that 1) the algorithms and strategy selected for the OSI SAF single sensor products have a high success rate and manage most of the time to return a vector and that 2) the multi platform merging strategy is efficient in populating the output grid.

As in Ezraty et al. 2008, it can be noted that the density curves sharply drop on both sides of the distribution period, indicating that the quality of the dataset is very much degraded before onset of freezing and after onset of melting. This behaviour is however not symmetrical during the month preceding (September) and the one following (May) the distribution period. Moreover, there is a clear difference between the behaviour of the three single sensor products. For example, this graph points towards a possible lengthening of the distribution period for the AMSR-E (37GHz) and ASCAT products but not for SSM/I (85 GHz). Approximately 10 (20) days could probably be gained in September (May) for those two products.

Similar effects can be observed from Figure (6) which displays the temporal evolution of

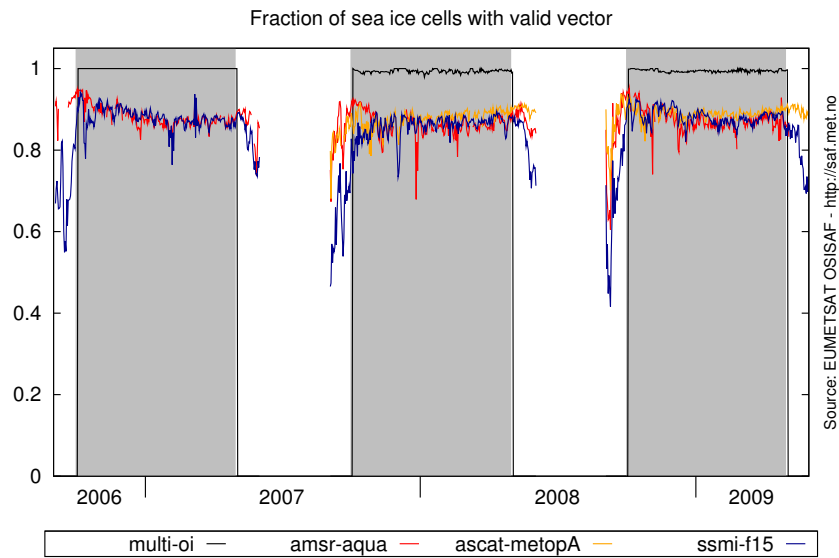


Figure 5: Temporal evolution of the density of valid vectors over the sea ice with time from 1<sup>st</sup> September 2006 to 31<sup>st</sup> May 2009.

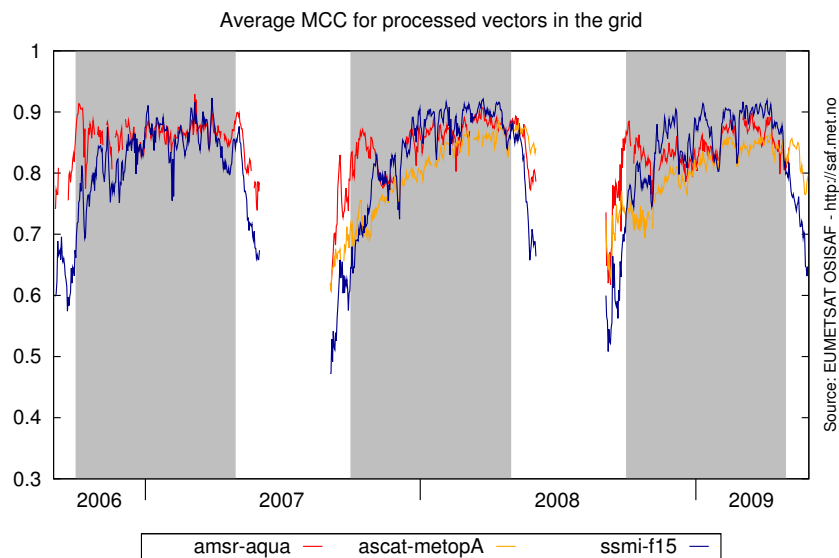


Figure 6: Temporal evolution of the average value of the MCC for computed vectors over the sea ice with time from 1<sup>st</sup> September 2006 to 31<sup>st</sup> May 2009.

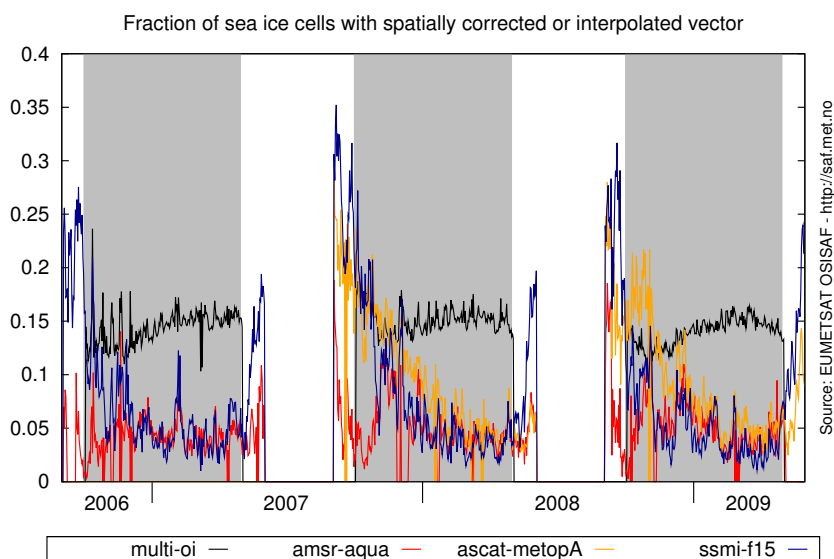


Figure 7: Temporal evolution of the density of spatially corrected (single sensor datasets) and interpolated (multi sensor dataset) vectors from 1<sup>st</sup> September 2006 to 31<sup>st</sup> May 2009.

the average for the Maximum Cross Correlation value of computed vectors (only for single sensor products, the multi-sensor product does not rely on image correlation processing). This average value is rather stable throughout the distribution period but drops outside this temporal domain.

Figure (7) displays the temporal evolution of the fraction of vectors that were not retrieved at the first CMCC processing and needed a correction step to take into account the spatial homogeneity constraint of the neighbouring vectors in the grid (single sensor products only, red, yellow and blue curves). This neighbourhood-based correction step is described in the PUM and the ATBD. Most of the time, this density is quite low. Around 5 to 10 % of the vectors in the output grid are concerned with this correction step. Outside the distribution period, and especially during September months, this value reaches 20 to 25 %, with worst conditions for SSM/I. The single sensor products based on ASCAT and AMSR-E seem to hold rather good densities during the May months.

Still on Figure (7), the black curve shows the fraction of the vectors in the multi-sensor grid that are obtained by spatial interpolation and, thus, not by one of the single-sensor datasets. This value is stable around 15 % all along the period. This number is mostly explained by the extent of the polar observation hole that is filled by spatial interpolation in the multi-sensor product only.

The current dissemination period from October throughout April thus seems like a *secure* period that might be later extended. In any case, the temporal behaviour in Figure (5) must first be validated on several years and linked to data quality.

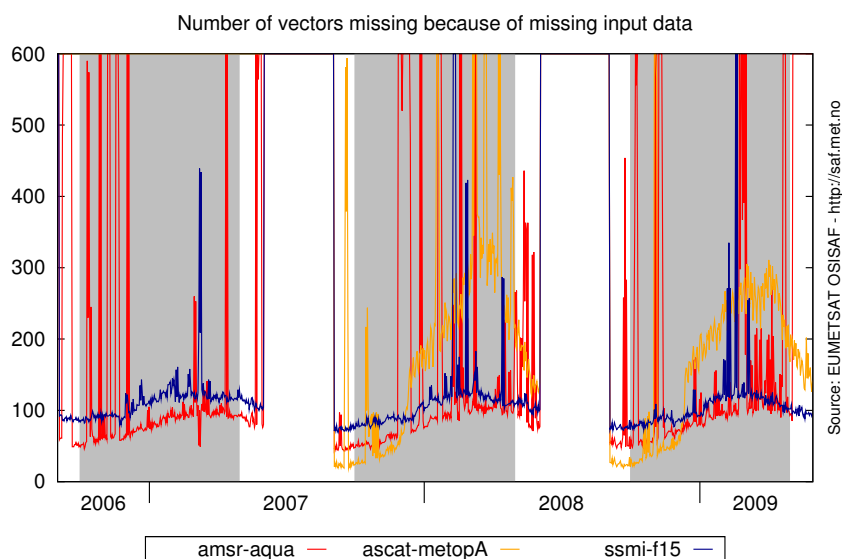


Figure 8: Temporal evolution of the number of missing vectors that are due to missing input swath data from 1<sup>st</sup> September 2006 to 31<sup>st</sup> May 2009.

## 5.2 Availability of input swath data and impact for use of the products

In chapter 4, we concluded that the product from AMSR-E instrument was of better quality than the others. Figure (8) displays the temporal evolution of the number of grid locations with missing ice drift vector when the failure is due to missing input data.

The curves are never zero. This is due to the polar observation hole (area of everlasting missing data) which hinders the retrieval of ice drift vectors at very high latitude. The polar observation hole is larger for SSM/I than for AMSR-E and even smaller for ASCAT. Typically, around 50 daily drift vectors are missing on the SSM/I product grid close to North Pole. This number is reduced to around 30 for AMSR-E. The ASCAT product only has 20 such missing vectors. Those numbers explain the ranking of the curves at the very beginning of the period, until about 1<sup>st</sup> December.

On Figure (8), the temporal signal for the AMSR-E product reveals spikes in the red curve. Those increase to more than 800 missing vectors occur when not a single swath is available as input to the processing chain. As a result, the single sensor ice drift product grid on that date is empty and disseminated as is. Such events occur less often for the SSM/I 'F15' platform. A totally missing daily coverage has a strong impact on the product's availability as the daily image is missing both as the start and end image of a product. Apart from totally missing products, users of the AMSR-E ice drift dataset should also be prepared to handle daily products with only partially filled grid.

The rather high values for ASCAT have another explanation. The curve for this product steadily increase from 1<sup>th</sup> December to 15<sup>th</sup> March before stabilizing and decreasing again by late April. In March, the number of missing vectors in the ASCAT grid is twice the one of AMSR-E for SSM/I. An analysis of the daily coverage of ASCAT swath data reveals that

---

several areas of the Northern Hemisphere are not imaged every day by ASCAT, particularly at moderate latitudes (Bering Sea, Hudson and Baffin Bay, etc...). Those areas are covered as the ice extent grows from December to March and ice motion vectors are successfully processed from AMSR-E or SSM/I that have a much better (almost complete) daily coverage but not from ASCAT. The graph would have been different if we had chose to only monitor the Arctic Ocean for which ASCAT coverage is complete.

## 6. Conclusion

This report deals with the validation and temporal monitoring of the OSI SAF 48h ice drift product from passive and active microwave satellite data. The region under study is the Arctic Ocean and the validation period runs for distribution years 2006-2007, 2007-2008 and 2008-2009: from October, 1<sup>st</sup> to April, 30<sup>th</sup>.

After having presented the data that constitute our reference dataset (mainly GPS in-situ trajectories) we introduced the validation strategy and, particularly, two ways of collocating the datasets: 2D which considers uniform start and end time at *1200 UTC* for all vectors and 3D which makes use of the extra time information available in the product file.

Results are analyzed from various graphs and statistics and conclude that the OSI SAF ice drift parameters  $dX$  and  $dY$  are mostly unbiased and that their statistical error probability distributions can be well represented by uncorrelated bivariate normal PDFs. Quantitative estimates of the terms entering  $C_{obs}$ , the error covariance matrix are provided in separate tables for the 2D and 3D collocation/usage.

Those tables confirm that the AMSR-E instrument gives the best ice drift vectors, with standard deviations (on  $dX$  and  $dY$ ) only slightly less than 3 km. The datasets from other sensors (SSM/I and ASCAT) have uncertainties level of around 4 – 4.5 km. SSM/I 'F15' seems to provide better results than the other DMSP platforms, F13 and F14 (not shown). Bias levels are very low in comparison.

As expected, the uncertainty level is slightly raised when the pixel varying time information is ignored (2D collocation). However, the standard deviations are only enhanced by few hundred meters. The multi sensor dataset is the one presenting least dependence on this extra time information.

It is worth mentioning that those validation statistics are matching the *threshold* and *target* accuracy requirements as specified in the Product Requirement Document CDOP PRD for OSI-405 product. The *threshold (target)* accuracy is 10 (5) km standard deviation. The *optimal* accuracy is defined as 2 km. This latter value might be reached by the AMSR-E product during selected periods of time (e.g. during the core of the winter season) but not on a yearly average validation exercise.

In a last chapter, temporal monitoring graphs are introduced which document that the chosen distribution period (similar to the one at IFREMER) is a 'safe' period and that it might be possible to extend it for some weeks, especially for the AMSR-E and ASCAT products. This will require more investigation, and particularly to conduct seasonal or monthly validation exercise over several years of data.

The attention of the interested user is finally drawn on the fact that the AMSR-E product is fairly less stable in its availability as input swath data are quite often missing or delayed. Near-real-time users might want to develop a strategy combining the AMSR-E dataset with, at least, a second product like SSM/I (F15) or ASCAT. Alternatively, the merged, multi-sensor

---

product can be selected but it remains, on average, less accurate than pure AMSR-E.

This report is a living document that will be updated when new sensors are introduced in the OSI SAF ice drift production chain as well as when the validation period is extended or when new data sources are available for inclusion in the reference dataset. The latest version of the present report and Product User Manuals are always available from the OSI SAF Ice web portal: <http://saf.met.no> or by contacting the author.

## References

CDOP PRD (2009, January). *Ocean and Sea Ice SAF CDOP Product Requirement Document*.

Ezraty, R., F. Girard-Ardhuin, and J.-F. Piollé (2007, February). Sea ice drift in the central Arctic estimated from SeaWinds/QuikSCAT backscatter maps – User’s manual. v2.2, CERSAT, IFREMER, France.

Ezraty, R., F. Girard-Ardhuin, and J.-F. Piollé (2008, April). Sea ice drift in the central Arctic combining QuikSCAT and SSM/I sea ice drift data – User’s manual. v3.0, CERSAT, IFREMER, France.

Haarpaintner, J. (2006, January). Arctic-wide operational sea ice drift from enhanced-resolution Quikscat/SeaWinds scatterometry and its validation. *IEEE Transactions on Geoscience and Remote Sensing* 44(1), 102–107.

Kwok, R., A. Schweiger, D. A. Rothrock, S. Pang, and C. Kottmeier (1998, April). Sea ice motion from satellite passive microwave imagery assessed with ERS SAR and buoy motions. *Journal of Geophysical Research* 103, 8191–8214.

Lavergne, T. and S. Eastwood (2010, March). Low resolution sea ice drift Product User’s Manual – v1.4. Technical Report SAF/OSI/CDOP/met.no/TEC/MA/128, EUMETSAT OSI SAF – Ocean and Sea Ice Sattelite Application Facility.

Lavergne, T., S. Eastwood, H. Schyberg, and L.-A. Breivik (2008, October). Ice drift monitoring from low resolving sensors: an alternative method and its validation against in-situ data. Report MERSEA\_WP02\_METNO\_STR\_005\_1A, MERSEA – Marine EnviRonment and Security for the European Area.

Lavergne, T., S. Eastwood, H. Schyberg, and L.-A. Breivik (2009, April). Algorithm Theoretical Basis Document for the OSI SAF low resolution sea ice drift product – v1.2. Technical Report SAF/OSI/CDOP/met.no/SCI/MA/130, EUMETSAT OSI SAF – Ocean and Sea Ice Sattelite Application Facility.

Lavergne, T., M. Voßbeck, B. Pinty, T. Kaminski, and R. Giering (2006). Evaluation of the two-stream inversion package. EUR 22467 EN, European Commission – DG Joint Research Centre, Institute for Environment and Sustainability.

Wiebe, H., G. Heygster, and L. Meyer-Lerbs (2008, October). Geolocation of AMSR-E data. *IEEE Transactions on Geoscience and Remote Sensing* 46, 3098–3103.